# Robust excitons inhabit soft supramolecular nanotubes

Dörthe M. Eisele[a,1], Dylan H. Arias[a], Xiaofeng Fu[b], Erik A. Bloemsma[c], Colby P. Steiner[a], Russell A. Jensen[a], Patrick Rebentrost[d], Holger Eisele[e], Andrei Tokmakoff[f], Seth Lloyd[d], Keith A. Nelson[a], Daniela Nicastro[b,1], Jasper Knoester[c,1], and Moungi G. Bawendi[a,1]

[a]Center for Excitonics and Department of Chemistry and [d]Department of Mechanical Engineering, Massachusetts Institute of Technology, Cambridge, MA 02139; [b]Biology Department, Rosenstiel Basic Medical Science Research Center, Brandeis University, Waltham, MA 02454; [c]Institute for Theoretical Physics and Zernike Institute for Advanced Materials, University of Groningen, NL-9747 AG, Groningen, The Netherlands; [e]Institut für Festkörperphysik, Technische Universität Berlin, 103623 Berlin, Germany; and [f]Department of Chemistry, University of Chicago, Chicago, IL 60637

Contributed by Moungi G. Bawendi, May 30, 2014 (sent for review December 2, 2013)

**Nature's highly efficient light-harvesting antennae, such as those found in green sulfur bacteria, consist of supramolecular building blocks that self-assemble into a hierarchy of close-packed structures. In an effort to mimic the fundamental processes that govern nature's efficient systems, it is important to elucidate the role of each level of hierarchy: from molecule, to supramolecular building block, to close-packed building blocks. Here, we study the impact of hierarchical structure. We present a model system that mirrors nature's complexity: cylinders self-assembled from cyanine-dye molecules. Our work reveals that even though close-packing may alter the cylinders' soft mesoscopic structure, robust delocalized excitons are retained: Internal order and strong excitation-transfer interactions—prerequisites for efficient energy transport—are both maintained. Our results suggest that the cylindrical geometry strongly favors robust excitons; it presents a rational design that is potentially key to nature's high efficiency, allowing construction of efficient light-harvesting devices even from soft, supramolecular materials.**

supramolecular assembly | self-assembled excitonic nanoscale systems | photosynthesis | exciton theory | light-harvesting antennae systems

The most remarkable materials that demonstrate the ability to capture solar energy are natural photosynthetic systems such as those found in primitive marine algae and bacteria (1–10). Their light-harvesting (LH) antennae are crucial components, because they absorb the light and direct the resulting excitation energy efficiently to a reaction center, which then converts these excitations (excitons) into charge-separated states (1, 4, 11, 12). Although the noncovalent interactions that link the individual molecules within the LH antennae are weak, the excitation transfer interactions between the molecules are relatively strong; new excited states, so-called Frenkel excitons (13), are generated that are delocalized over a number of molecules (1). These delocalized excitons are key to nature's efficiency and are therefore of high interest (14–20).

To create such efficient LH systems, nature assembles molecular subunits into individual supramolecular structures, which are then further assembled into close-packed superstructures (1, 4, 7–10, 12, 21). This hierarchical assembly is a generic motif of nature's photosynthetic systems. As with natural systems, assembling artificial LH devices from supramolecular structures will require close packing into hierarchical assemblies to maximize the amount of absorbed light (19). Therefore, key to our ability to tune materials properties for efficient LH applications is a basic understanding of the role of each level of the hierarchy: from the individual molecule, to the individual supramolecular building block, to the close-packed assembly. Whereas the role of the individual molecules in the excitonic properties of the building blocks is well-studied (1, 7–10, 20, 22–37), the effect of structural hierarchy remains an open question because the system's soft structure may be easily altered upon close packing: Do the excitonic properties change as the individual supramolecular structures assemble into a close-packed superstructure? In other words, can we simplify the materials properties as a superposition of the properties of the building blocks or does their close packing require a different interpretation?

In nano-science size and shape have important impact on a system's properties (1). Interestingly, one of nature's most spectacular class of LH antennae systems that was found in green sulfur bacteria (7–10, 15, 34, 38, 39) uses cylindrical-shaped geometries as a basic design principle for their supramolecular building blocks (7–10). Does nature gain an advantage from using cylindrical-shaped rather than simple sheet-like geometries as a design principle for one of its most efficient LH antennae?

The ultimate next step is to elucidate the impact of hierarchical assembly on excitonic properties that are critical to the system's efficiency. However, it is difficult to disassemble nature's hierarchical structures into their supramolecular building blocks to study and understand the impact of hierarchical assembly. A promising approach would be to use a well-defined model system for which basic investigations are possible in every single step on the hierarchical assembling process.

## Significance

**The scientific community has been broadly inspired by tiny deep-sea bacteria, the green sulfur bacteria, that are able to harvest minute amounts of incoming sunlight with exquisite efficiency. Nature's masterpiece consists of soft, cylindrical-shaped, supramolecular structures that are densely packed in superstructures. Only little is known about the fundamental processes that govern nature's efficiency. Here we unravel, for the first time to our knowledge, the impact of structural complexity through the use of a model system akin to that found in nature, focusing on the properties that are prerequisite for nature's efficient light harvesting. Our work suggests that the cylindrical geometry presents a rational design that may be key for protecting the system's quantum properties upon dense packing.**

Author contributions: D.M.E. and M.G.B. developed and guided the project; D.M.E. prepared shock-frozen samples for cryo-EM/ET, prepared samples for nonlinear spectroscopy, and performed linear spectroscopy experiments; D.H.A. performed linear dichroism and nonlinear spectroscopy experiments and data analysis with input and support from D.M.E. and C.P.S. and guidance from A.T. and K.A.N.; X.F. recorded and processed cryo-EM/ET data; D.M.E., X.F., and D.N. analyzed cryo-EM/ET data; E.A.B. performed spectral simulations in collaboration with D.M.E. supervised by J.K.; R.A.J. built the fast-acquisition absorption spectrometer and performed flash-dilution measurements with D.M.E.; P.R. performed exciton dynamic simulations in collaboration with D.M.E and S.L.; H.E. provided fundamental contributions to the discussion on the structure analysis and simulated illustrations for the bundle structure; all authors provided fruitful discussions and interpretations of the data and analyses; J.K. provided essential interpretation of optical data, particularly in the context of exciton theory; and D.M.E., S.L., J.K., and M.G.B. wrote the paper, with input from all authors.

The authors declare no conflict of interest.

Freely available online through the PNAS open access option.

[1]To whom correspondence may be addressed. Email: Eisele@ccny.cuny.edu, Nicastro@brandeis.edu, J.Knoester@rug.nl, or MGB@mit.edu.

This article contains supporting information online at www.pnas.org/lookup/suppl/doi:10.1073/pnas.1408342111/-/DCSupplemental.

In this paper we realize the comprehensive investigation of an artificial model system that mirrors the complexity of natural LH antennae: artificial LH nanotubes (LHNTs) of amphiphilic cyanine dye molecules (40) self-assembled into a cylindrical geometry with a diameter on the order of 10 nm (41) and a length that may extend to micrometers (29, 42). We show that these LHNTs can complete the hierarchical assembly by further assembling into bundled LHNTs that consist of close-packed cylindrical building blocks. We use a cross-disciplinary approach that combines rigorous structural characterization along with optical spectroscopy through complementary experimental methods—electron microscopy techniques, linear and nonlinear optical spectroscopy, flash dilution, and redox-chemistry—and theoretical simulations. This approach allows for a direct comparison of the excitonic properties originating from the individual supramolecular building blocks and from the close-packed building blocks. The observed spectral changes upon close packing can be explained by minor changes within the supramolecular structure of the building blocks. In contrast, we find that the properties prerequisite for efficient excitation energy transport are maintained through close packing: a high degree of internal order, strong excitation transfer interactions, and large exciton delocalization, evoking the term "robust excitons." Our results suggest that the cylindrical geometry presents a rational design that is potentially key for constructing efficient LH systems from artificial supramolecular materials, potentially by minimizing perturbations of the excitonic properties upon formation of hierarchical structures.

In particular, we study LHNTs (31) composed of the amphiphilic cyanine dye C8S3 (Fig. 1*A*, *Inset* and *Materials and Methods*). Cryo-electron microscopy (cryo-EM) shows that freshly prepared LHNTs in water/methanol solution are well separated from one another (Fig. 1 *A* and *B*), consistent with previous work (31, 41, 43). These LHNTs present a homogeneous ensemble with a remarkably uniform supramolecular structure (29) and are composed of two concentric cylinders, as schematically illustrated in Fig. 1*C*, separated by about 4 nm: an inner cylinder with a diameter of ∼6 nm (43) and an outer cylinder with a diameter of ∼13 nm (41, 43). Cryo-EM reveals that the double-walled LHNTs further self-assemble over time into bundled nanotubular structures (Fig. 1*D*). Bundles are either straight or twisted (Fig. 1*E* and *SI Appendix*, section 1).

Upon self-assembly into double-walled LHNTs the broad absorption band of the monomers (Fig. 1*F*) undergoes a large redshift of ∼80 nm (∼2,500 $cm^{-1}$), reflecting strong excitation transfer interactions between the molecular transition dipole moments of the molecular subunits (31). The narrowing of the absorption peaks relative to the monomer spectrum, so-called exchange narrowing (13), originates from the delocalization of the excitation over multiple molecular subunits. These delocalized excitations average out short-range monomer inhomogeneities. The exciton delocalization length is defined as the number of molecular subunits over which the excitation is delocalized. In addition, the cylindrical geometry gives rise to a complex pattern of absorption bands (25) that has previously been mapped onto the system's structure (Fig. 1*F*): Bands 1 and 3 mainly originate from the inner cylinder, whereas band 2 mainly originates from the outer cylinder (31). The narrow linewidth of low-energy band 1 suggests large exciton delocalization (23, 44).

Interestingly, monitoring the bundling process in real time by means of absorption spectroscopy (*SI Appendix*, section 2) shows that the double-walled LHNTs and the bundled LHNTs have different optical properties. Upon bundling the two main absorption bands of the double-walled LHNTs at 599 nm (band 1) and at 589 nm (band 2) disappear (Fig. 1*F*), and two new transitions grow in: a narrow band at 603 nm (I) and a broad band at 575 nm (II). We assign these two new bands to the bundled LHNTs. For the double-walled LHNTs (Fig. 1*F*), bands 1 and 2 are polarized primarily parallel to the cylindrical axis, whereas band 3 is polarized primarily perpendicular to it. For the bundled LHNTs (Fig. 1*F*), band I is primarily polarized parallel whereas the broad band II is primarily polarized perpendicular (*SI Appendix*, section 3).

## Morphological Structure

Cryo-electron tomography (45) (cryo-ET) allows visualization of the 3D structure of the bundled LHNTs. Fig. 2*A* shows one cryo-ET frame of a 3D reconstruction of bundles (*SI Appendix*, section 4; see also Movies S1 and S2). Fig. 2*B* depicts the iso-surface renderings of cryo-ET reconstructions of twisted and straight bundles. Fig. 2*C* shows a cryo-ET cross section averaged over the length of a twisted bundle. The iso-surface rendering of this twisted bundle is shown in Fig. 2*D* and reveals that this bundle consists of 12 hexagonally close-packed nano-tubular objects. On average, bundles consist of about 13 nano-tubular objects. Fig. 2*E* shows representative line scans taken perpendicular to the bundles, from straight bundles imaged by cryo-TEM (Fig. 1*D*) and from twisted bundles imaged by cryo-ET (Fig. 2*A*), revealing a center-to-center distance of 10 ± 1 nm (*SI Appendix*, section 5). This distance is too small to originate from the packing of the double-walled LHNTs shown in Fig. 1 *A* and *B*. Instead, this center-to-center distance is consistent with the packing of just the inner cylinders from the initially formed LHNTs, where each cylinder has a diameter of 6 ± 1 nm and a minimal distance to their neighboring cylinders of 4 ± 1 nm, which is the same as for the cylinder-to-cylinder distance in double-walled LHNTs, dictated by the spatial dimensions of the monomer's hydrophobic side chains (Fig. 1*A*, *Inset*). This structure of bundles of close-packed cylinders is schematically illustrated in Fig. 2*F*. Similar to the structure of the double-walled LHNTs, it is reasonable to expect that the bundles are surrounded by an outer envelope layer of self-assembled dye molecules that expose their hydrophilic heads to the aqueous solution. Our EM results suggest the inner cylinders of the double-walled LHNTs stay morphologically intact upon bundling and act as the building blocks to form close-packed hierarchical superstructures: bundled single-walled LHNTs encapsulated by an outer envelope layer.

## Absorption Spectra

At this point, it remains an open question whether the excitonic properties of the individual building blocks change as they assemble into bundles. This key question can be addressed directly by comparing the optical properties of the building blocks before and after bundling. To this end, experimental techniques are required that allow for identifying the spectral contributions of the building blocks without perturbing their nano-tubular morphology.

Oxidation chemistry (43) has been previously used with double-walled LHNTs as an elegant tool to identify the spectral contributions of the inner cylinder by selectively oxidizing the dye molecules in the outer layer and "turning off" their optical response (31). However, oxidation chemistry does not a priori select one layer over another because it is based on relative redox potentials rather than location within the hierarchical assembly (46, 47). Flash dilution (31) is a complementary method that can connect the relative positions of layers to the absorption bands. Flash dilution is expected to affect the system's outer layers, which are directly exposed to the solvent, to a greater degree than the system's inner and more protected regions. Unlike oxidation, flash dilution, by physically disrupting the supramolecular structure of the outer layers, may perturb the morphology of the remaining structure, changing its spectrum. The two methods together can, however, confidently isolate the optical spectrum of one layer over the other.

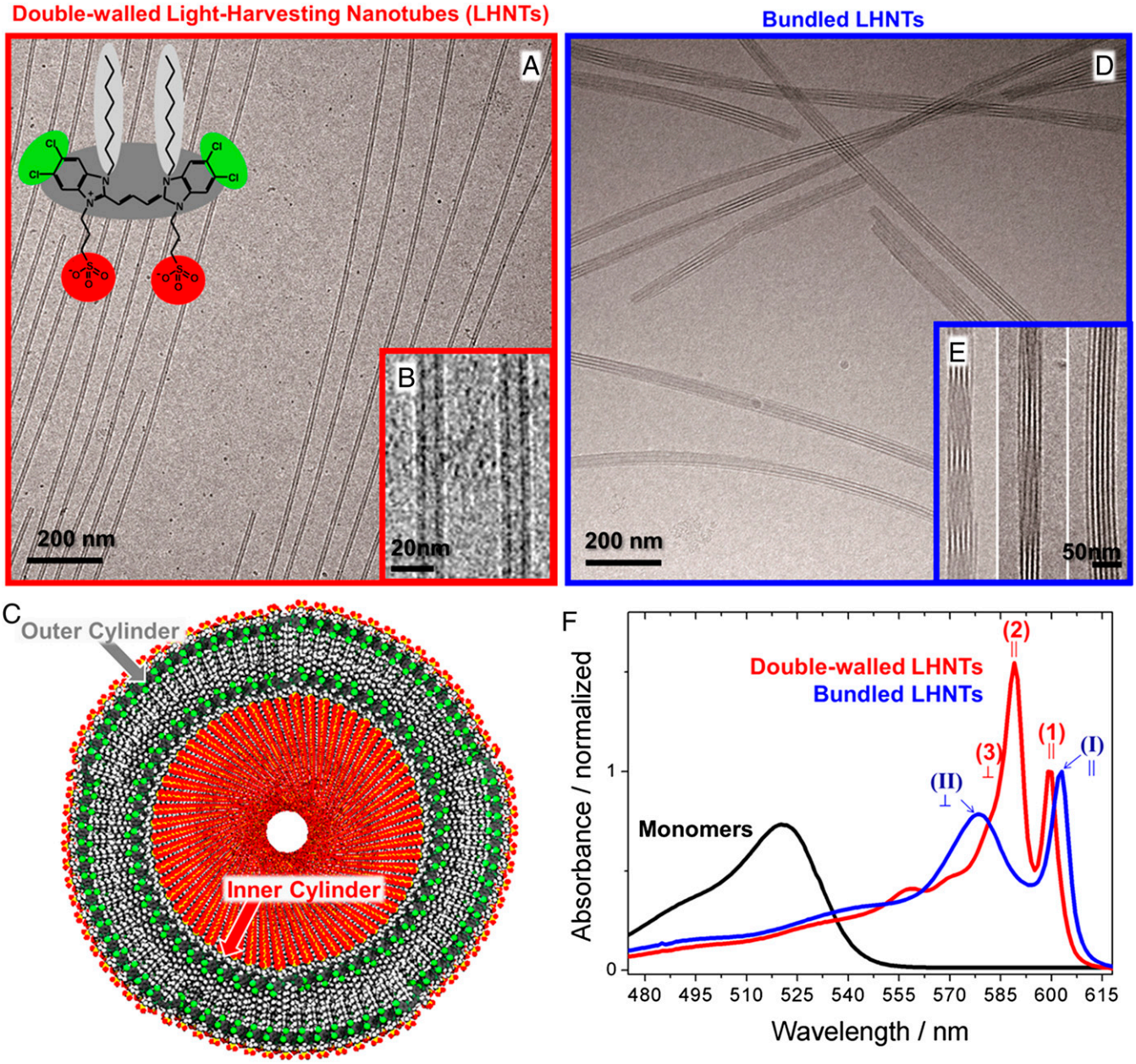


**Fig. 1.** Correlating morphological and optical properties. (*A*) Cryo-EM micrograph of double-walled LHNTs self-assembled from amphiphilic cyanine dye molecules (abbreviated as C8S3; *Materials and Methods*) with molecular structure in inset. (*B*) EM micrograph at higher magnification shows the double-walled nature of the LHNTs. (*C*) Schematic illustrates the LHNT consisting of two concentric cylinders self-assembled from C8S3 molecules (for clarity using only one molecule per unit cell) with the hydrophilic sulfonate groups (red) on the exterior, the hydrophobic alkyl chains (light gray) in the interior of the bilayer, and the cyanine dye chromophore (dark gray) in the middle. (*D*) Cryo-EM micrograph of bundled LHNTs in overview and (*E*) at higher magnification shows three examples of different morphologies: bundles with a straight morphology (right) and with increasing amounts of twist (middle and left), which is indicated by the Moiré pattern (i.e., alternating bands of sharp and blurred lines along the cylindrical axis). (*F*) Absorption spectra. Black: absorption spectrum of C8S3 dye molecules (monomers) dissolved in methanol. Red: absorption spectrum upon self-assembling of double-walled LHNTs prepared in water/methanol. Blue: absorption spectrum of bundles of LHNTs. || and ⊥ indicate polarization parallel and perpendicular to the cylinder axis, respectively. See text for transition labeling and *SI Appendix*, section 3 for polarization of the bands.

The time evolution of the absorption spectra upon flash dilution is shown in Fig. 3 *A* and *B* for double-walled LHNTs and bundled LHNTs, respectively. For double-walled LHNTs, band 2 vanishes completely (Fig. 3*A*), consistent with it originating from the outer cylinder, and there is a concomitant increase in the monomer absorption band at ∼520 nm. For the bundled LHNTs (Fig. 3*B*) bands I and II are largely unchanged but there is an increase in the monomer absorption band at ∼520 nm that can be attributed to preferentially disrupting the structure of the surrounding outer envelope layer (*SI Appendix*, section 6). This is consistent with bands I and II originating mainly from the bundled inner-cylinders. These results also suggest that the outer layer of bundled LHNTs contributes to the absorption spectrum not with narrow exciton bands but with a spectrally broad distribution of bands, consistent with an inhomogeneous supramolecular structure.

In contrast to flash dilution, chemical oxidation does not perturb the system's nano-tubular morphology as schematically

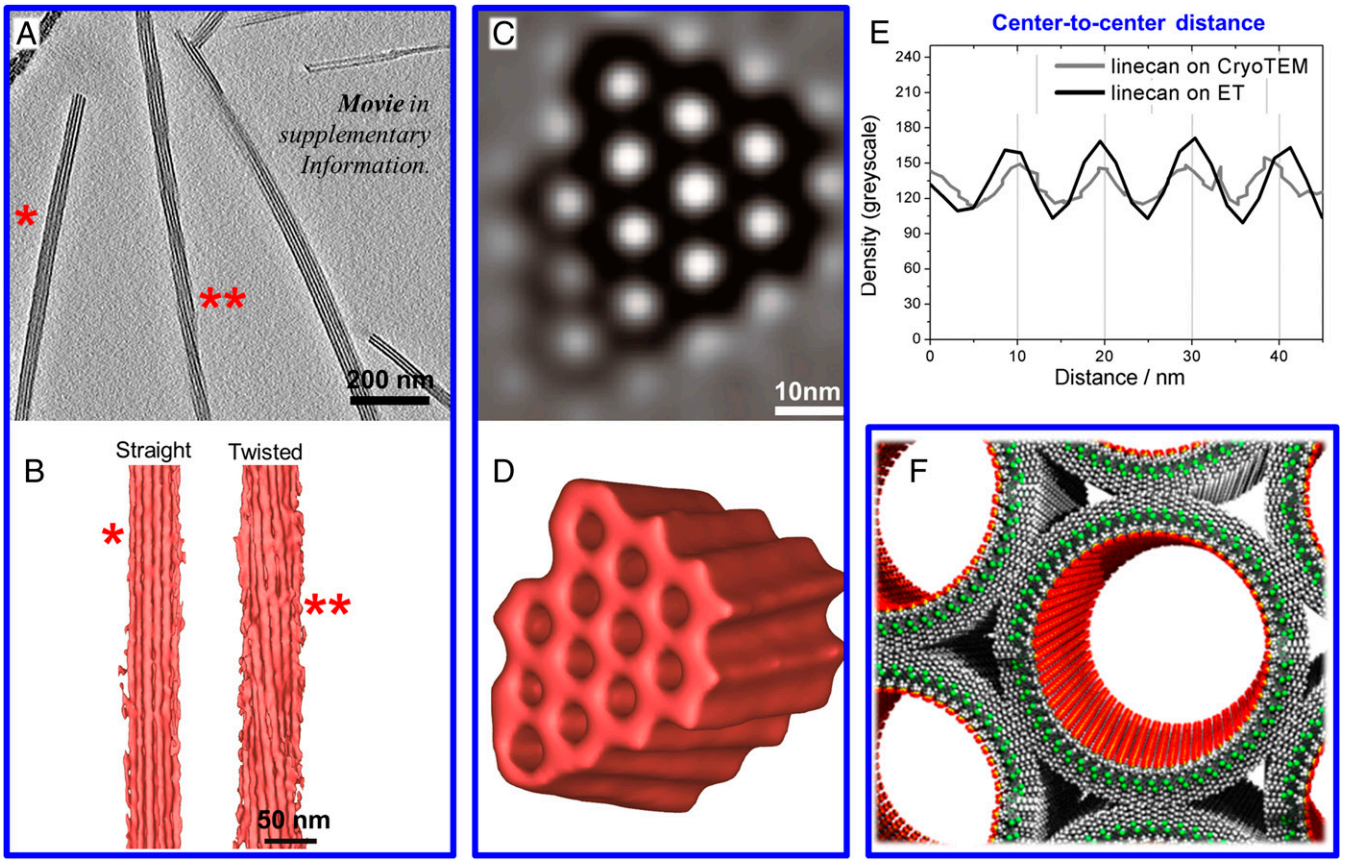


**Fig. 2.** Morphological structure of bundled LHNTs. (*A*) Representative slice through a cryo- ET of bundled LHNTs (see entire ET volume in Movies S1 and S2). (*B*) Iso-surface renderings of cryo-ET reconstructions of bundled LHNTs with straight (left) and twisted (right) morphologies (see also *SI Appendix*, sections 4 and 5). (*C*) Cryo-ET slice taken from an averaged cryo-ET showing a cross-sectional view of a twisted bundle (see also *SI Appendix*, sections 4 and 5). (*D*) Iso-surface rendering of a twisted bundle. (*E*) Representative line scans (*SI Appendix*, section 5) taken on cryo-EM (Fig. 1*D*) and cryo-ET (Fig. 2*C*) from twisted and straight bundles, respectively, revealing a center-to-center distance of 10 ± 1 nm. (*F*) Schematic illustrating bundle morphology: The inner cylinder of a double-walled LHNT (as illustrated in Fig. 1*C*) stays morphologically intact upon bundling and acts as a building block for the bundled LHNT system.

illustrated in Fig. 4*A*. Therefore, chemical oxidation can be used to identify the absorption spectrum of both the inner cylinder (building block) of the double-walled LHNTs and the bundled cylinders (*SI Appendix*, section 7), as depicted in Fig. 4*B*. The lowest energy transition band of the inner cylinder, band 1 at 599 nm, undergoes a minor red-shift upon bundling, band I at 603 nm, whereas most interestingly the narrow linewidth of this transition does not change significantly (Fig. 4*B*, *Inset*). This is particularly remarkable because the ensemble of bundles seemingly presents a significantly more inhomogeneous morphology compared with the well-defined inner cylinders of the double-walled LHNTs. The survival of the narrow linewidth of the lowest-energy exciton band upon hierarchical assembly reflects a preservation of a high degree of internal order and effectively unchanged exciton delocalization lengths, prerequisite conditions for efficient excitation energy transport. Despite the soft nature of the assembly owing to weak intermolecular forces between molecular subunits, the lowest-energy exciton properties are maintained even upon close packing, suggesting the term robust exciton.

The higher-energy transitions of the inner cylinder between 550 nm and 585 nm are replaced upon bundling with a broad band centered on 575 nm. These higher-energy transitions, although crucial for light absorption, are unlikely to affect energy transport processes, because their energy exceeds the lowest-energy excitons by considerably more than the thermal energy, even at room temperature. The question arises: What explains the spectral changes observed?

## Experiment vs. Theory

In general, the optical properties of a supramolecular structure are highly sensitive to the details of its molecular arrangement, and this arrangement is very sensitive to the details of the chemical environment surrounding the structure. Upon bundling, the building block is no longer homogenously encapsulated by the well-defined outer cylinder but instead is now part of a finite hexagonal lattice of other cylinders. Even though the bundling process apparently does not alter the cylinder's gross morphology, it may generate shifts in molecular transition energies owing to a changed environment or even alter the details of the cylinder's molecular arrangement. Theoretical simulations can be used as a tool for probing how structural changes can affect the system's optical properties, and in particular if changes in the details of the molecular arrangement can explain the spectral changes observed in Fig. 4*B*. These simulations consider the excitonic interactions between molecules, which are sensitive to their relative separations and orientations, and hence to their specific arrangement. The extended herringbone (EHB) structure (31) previously has been used to explain the absorption spectrum of the double-walled LHNTs' inner cylinder as shown in Fig. 4*C* (in red). Here, extensive simulations (Fig. 4*C*, in blue) show that, indeed, small changes of the inner cylinder's molecular arrangement (see the caption for Fig. 4) allow for the type of

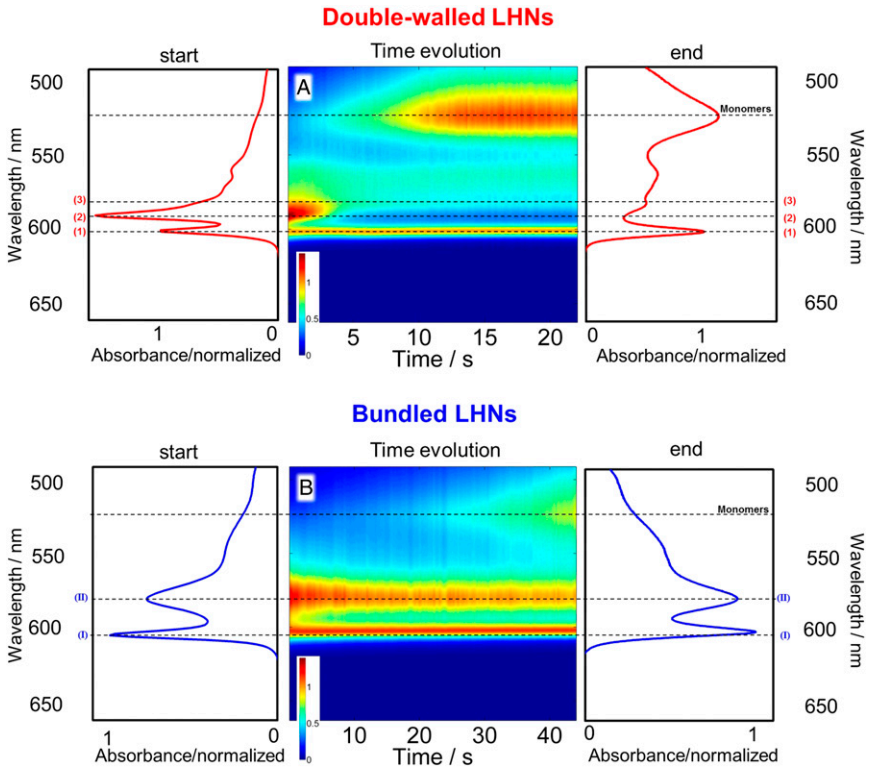


**Fig. 3.** Mapping exciton transitions to structure. Time evolution of the absorption spectra upon flash dilution of (*A*) double-walled LHNTs and (*B*) bundled LHNTs. In both cases the absorption features from the LHNTs decrease whereas the monomer feature at 520 nm increases. The increase in the monomer absorption can be attributed to preferentially disrupting the supramolecular structure in the system's outer regions. Accordingly, the spectral contributions that vanish can be assigned to the system's outer regions, whereas the remaining bands can be assigned to the inner cylinders.

spectral changes observed upon bundling. In particular, we can replicate the strong changes in the high-energy region while hardly affecting the low-energy region of ~600 nm. Moreover, we also found that a packing of double-walled LHNTs with reasonable variations in model parameters cannot explain the changes in the observed spectra (Fig. 4*B*), consistent with our morphological characterization. When simulating optical spectra of molecular aggregates, one often includes disorder in the molecular transition energies to account for the heterogeneous nature of these systems and their host media (23). The simulated spectra of the building block shown here have been calculated without including disorder because this facilitates comparison with the previous simulations for double-walled LHNTs (31). In addition, it was found that allowing for disorder does not change the main conclusion, namely, that the building block's spectral changes upon bundling can be understood from both relatively small rearrangements in the inner cylinder's molecular packing and an absence of a surrounding outer cylinder. Nevertheless, it is reasonable to assume that disorder also plays a role in these supramolecular aggregates and contributes (partly) to the width of the absorption bands and leads to exciton localization, which is of crucial importance in the optical dynamics of supramolecular aggregates. To gain some qualitative insight into the behavior of the excitons in the ~600 nm region under the influence of inhomogeneities, we considered Gaussian energetic disorder in the molecular transition energies and simulated the excitation density of the molecular subunits in the cylinder. Fig. 4*D* shows a typical example of this excitation density for an exciton in the ~600-nm band region using a maximum value for the disorder strength (see the caption for Fig. 4). We find that the exciton in the ~600-nm region is still delocalized over hundreds (up to ~1,000) molecules and extends in a helical direction around the cylinder, consistent with the direction of the strongest intermolecular interactions. We also performed simulations of double-walled LHNTs, allowing for various types of heterogeneity, such as Gaussian energy disorder or a hexagonal modulation of the transition energies originating from the bundle's packing. We found that none of these models could explain the spectral changes upon bundling.

## Excitonic Coupling

Nature's solution for highly efficient LH is a hierarchy of length scales accompanied by a hierarchy of excitonic coupling strengths. Combining 2D electronic spectroscopy (2D ES), as explained in *SI Appendix*, section 8, with knowledge of the structural origin of exciton bands and their polarizations allows elucidating the hierarchy of excitonic couplings in the LHNTs. A collinear experiment with pump and probe both polarized parallel to the cylindrical axis probes correlations between exciton transitions with polarization oriented along the cylindrical axis, here between bands 1 and 2 in the double-walled LHNTs. By contrast, a cross-linear experiment can reveal correlations between mutually perpendicular transitions. Two-dimensional ES absorptive spectra at zero waiting time for both double-walled LHNTs and bundled LHNTs are shown in Fig. 5 *A* and *B* and Fig. 5*C*, respectively. In the collinear 2D spectrum of the double-walled LHNTs (Fig. 5*A*) the diagonal peaks correspond to the features observed in the linear absorption spectrum. A weak cross-peak between bands 1 and 2 indicates weak excitonic coupling between the inner and outer cylinder, which is consistent with previous redox chemistry experiments on this system (31) and with previous pump-probe spectroscopy (48) and 2D ES on a similar nanotubular system (49). In contrast, the cross-linear 2D spectrum (Fig. 5*B*) shows a high-amplitude cross-peak at zero waiting time between bands 1 and 3 of the inner-cylinder—reflecting a strong correlation between those two transitions, or,

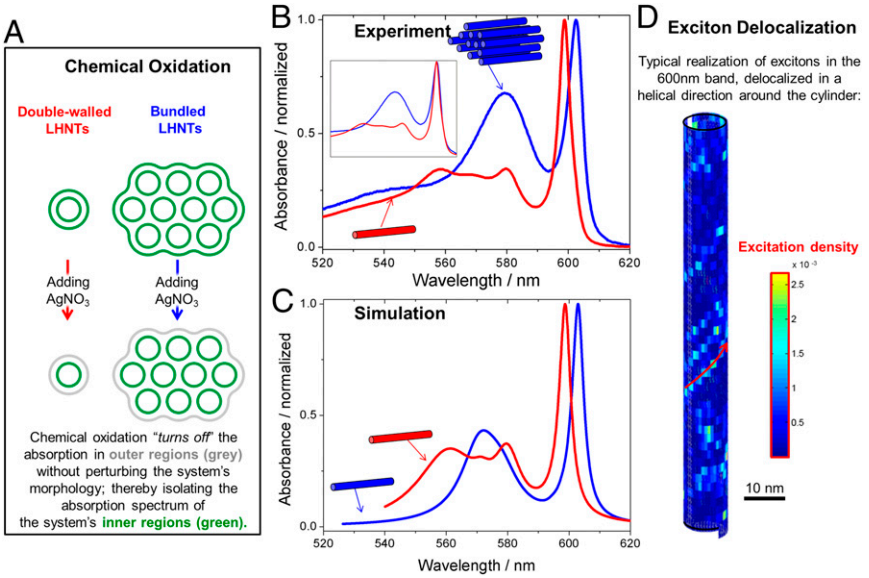


**Fig. 4.** Absorption spectra of building blocks and exciton delocalization. (*A*) Schematic: In contrast to flash dilution, chemical oxidation upon adding $AgNO_3$ does not perturb the mesoscopic structure of the LHNTs but preferentially eliminates absorption in regions that are preferentially oxidized. (*B*) Experiment: Chemical oxidation in solution used as a tool to isolate the absorption spectrum (red) of individual building blocks (inner-cylinders of double-walled LHNTs in the presence of oxidized outer-cylinders) and to isolate the absorption spectrum (blue) of bundled building blocks (bundled inner-cylinders in the presence of the oxidized surrounding outer layer). (*Inset*) Both spectra have been overlaid showing that upon bundling the line width of the lowest energy exciton mode does not change significantly. (*C*) Simulation: Simulated absorption spectrum (red) using the EHB structural model proposed previously for the inner cylinders of double-walled LHNTs (31) and the absorption spectrum (blue) calculated for an inner-cylinder upon slight modification of the packing parameters; here, the monomer's tilt angle was decreased from 23.6° to 22.8°, the rotation angle was changed from 25.6° to 17.0°, and the wrapping angle was reduced from 53.7° to 47.0° (see ref. 31 for definitions). Both spectra are calculated without any disorder present and the transitions have been broadened by Lorentzian lineshapes to facilitate comparison with the experimental results. The simulations show that minor changes in the details of the molecular packing can qualitatively explain the experimentally observed spectral changes—including polarization—upon bundling. (*D*) Exciton delocalization: Typical example of the excitation density of the molecules (absolute value squared of the exciton wavefunction coefficients) in an inner cylinder, consisting of about 8,000 molecules organized in the EHB structural arrangement, in the presence of disorder in the molecular transition energies (see also *Materials and Methods*). The disorder strength (250 $cm^{-1}$) was obtained assuming that the lowest energy bandwidth at 600 nm completely derives from inhomogeneous broadening, thus providing an upper limit on the amount of disorder. The simulations reveal that the exciton in the 600-nm band for this disorder strength is delocalized over typically hundreds (up to ~1,000) of molecules, spread in a helical manner around the cylinder in the direction of the strongest intermolecular interactions.

in other words, that they have a common ground state and are part of the same excitonic system. Note the absence here of the diagonal peak corresponding to band 3: The signal from this transition is not observed here because its polarization is perpendicular to the detection polarization. Therefore, the high-amplitude cross-peak in the cross-linear 2D spectrum of the double-walled LHNTs (Fig. 5*B*) is simply a consequence of the fact that both transitions belong to the same cylinder and share the same ground state; exciting one transition causes a bleaching signal of the other one.

Electronic coupling between nanoscale systems depends intimately on their distance. The wall-to-wall distance in the double-walled LHNTs and the wall-to-wall distance of neighboring cylinders in the bundled LHNTs are both dictated by the spatial dimension of the hydrophobic chains that separate them. Accordingly, it is reasonable to assume the cylinder-to-cylinder coupling to be similarly weak in both systems. The high-amplitude cross-peak in the cross-linear 2D spectrum of the bundled LHNTs (Fig. 5*C*) reflects the fact that here as well both transitions belong to the same cylinder: The strong excitonic correlations within the building blocks are retained upon their close packing.

## Summary and Conclusions

In an effort to mimic nature's highly efficient LH antennae, it is important to elucidate the role of each level of their structural hierarchy: from molecule, to supramolecular building block, to close-packed building blocks. This work constitutes a systematic study that elucidates the effect of structural hierarchy on critical excitonic properties in supramolecular systems. We accomplish this by using a cross-disciplinary approach to fully characterize an artificial analog to the natural LH antenna systems of the green sulfur bacteria, morphologically and optically, and complement this with theory. In particular, we have elucidated how the excitonic properties change as the individual supramolecular structures assemble into close-packed superstructures. Specifically, we have shown that the inner cylinders of double-walled LHNTs, self-assembled from the synthetic cyanine dye C8S3 in water/methanol solution, act as well-defined building blocks to form close-packed hierarchical superstructures: bundled single-walled LHNTs encapsulated by an outer envelope layer. Our work demonstrates that these LHNTs are an excellent model system for studying hierarchically structured excitonic systems. As with natural LH complexes, our model system exhibits a hierarchy of length scales accompanied by a hierarchy of excitonic coupling strengths. On the length scale of the distance between the inner cylinders and outer cylinders of the double-walled LHNTs, our experiments demonstrate relatively weak excitonic coupling, which is consistent with previous work (31, 49). In contrast, on the shorter length scale of the molecular subunits within the cylinders, strong excitonic correlations are retained upon close packing. Most interestingly, our combined experimental and theoretical approach reveals that the properties prerequisite for efficient excitation energy transport are preserved upon bundling: a high degree of internal order, strong excitation transfer interactions, and a large exciton delocalization, thus evoking the term robust excitons. This suggests that, even upon close packing, the inner cylinders of double-

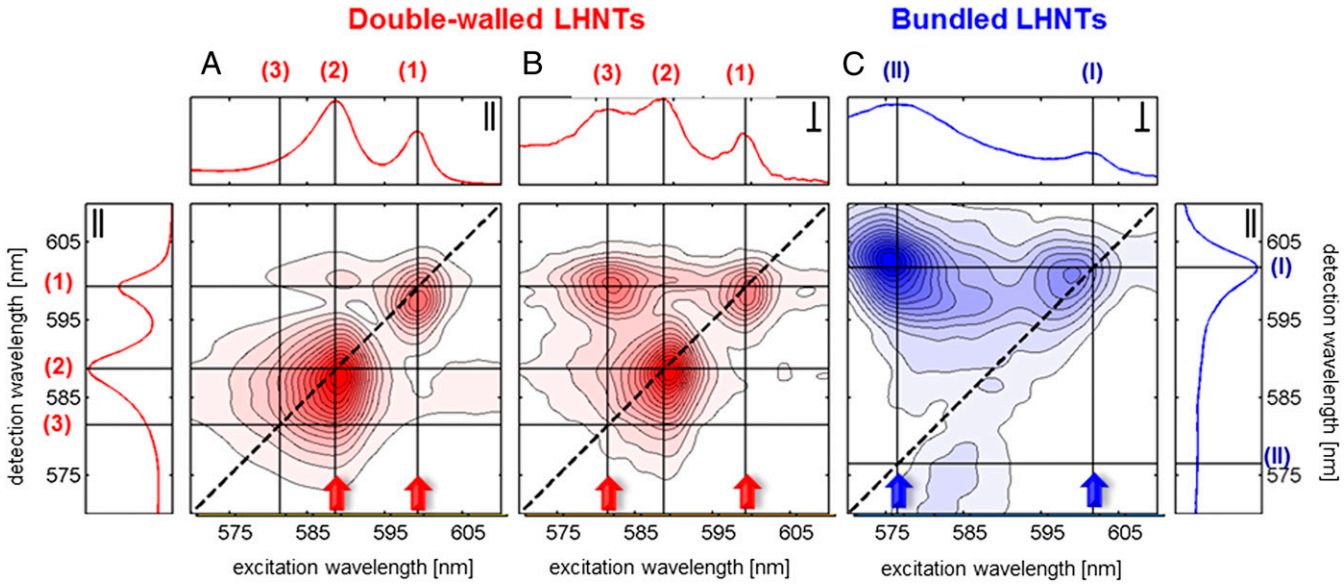


**Fig. 5.** Correlation of exciton transition bands. (*A*) Two-dimensional electronic correlation spectroscopy (2D ECS) of aligned double-walled LHNTs with excitation and detection polarized parallel to the cylindrical axis. A weak cross-peak is evident between transitions 1 and 2 indicating weak excitonic coupling between the inner cylinder and the outer cylinder. (*B*) Cross-polarized 2D ECS with perpendicularly polarized excitation and parallel polarized detection. A high-amplitude cross-peak between transitions 1 and 3 indicates strong excitonic correlations within the inner cylinder (i.e., the building block). (*C*) Cross-polarized 2D ECS of aligned bundled LHNTs with perpendicularly polarized excitation and parallel polarized detection. A high-amplitude cross-peak between transitions I and II indicates retained strong excitonic correlations within the building blocks even upon their close packing. The red and blue arrows point at the excited transitions of interest.

walled LHNTs hold the potential for efficient energy transport and therefore may act as "exciton highways." Densely packed superstructures in artificial LH systems, as in natural systems, increase the system's order and concentrate light absorption. Accordingly, close-packed one-dimensional building blocks may potentially form "exciton superhighways," as illustrated in Fig. 6. Although it is possible to obtain conditions for directed excitation energy transport with 2D building blocks (such as sheets) by reducing dimensionality using modulations of the assembly's energy landscape (*SI Appendix*, section 9), our results show that close packing of soft supramolecular assemblies with cylindrical geometry provides an elegant way to direct excitation energy without additional modifications. We speculate that the cylindrical geometry may play a key role in minimizing perturbations of the excitonic properties upon formation of hierarchical structures. Natural LH systems require robustness; our work shows that the design principle of cylindrical-shaped building blocks seems to favor robustness even though close packing may alter the cylinders' soft mesoscopic structure. Our results suggest that the cylindrical geometry presents a rational design that is potentially key to nature's high efficiency, allowing construction of efficient LH devices even from soft supramolecular materials. We speculate that in natural LH systems, such as those found in the green sulfur bacteria, cylindrical-shaped geometries protect the exciton modes that are responsible for efficient excitation energy transport properties. We predict that the robust excitons that inhabit cylindrical building blocks make such building blocks

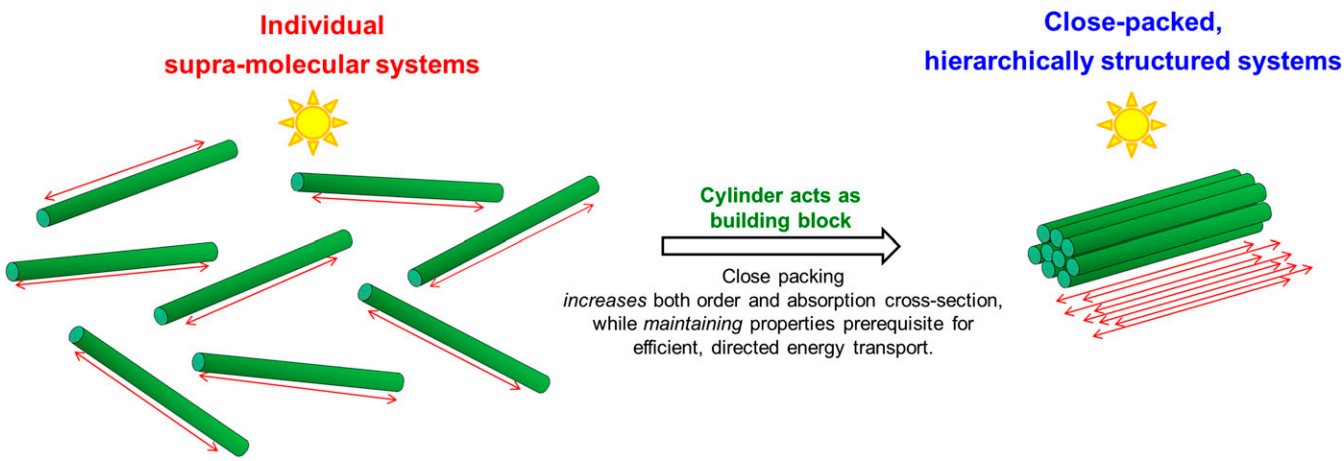


**Fig. 6.** Close packing of soft quasi-1D nano-structures with robust excitonic properties. As with natural systems, formation of LH systems from artificial building blocks requires their assembly into densely packed superstructures to increase the system's order and to concentrate the absorption, both prerequisites for efficient and directed energy transport.

attractive in the design of efficient opto-electronic devices constructed from supramolecular materials.

## Materials and Methods

**Preparation of Light-Harvesting Nanotubes.** The amphiphilic cyanine dye derivative 3,3′-bis(2-sulfopropyl)-5,5′,6,6′-tetrachloro-1,1′-dioctylbenzimidacarbocyanine (C8S3, molecular weight 902.8 g·mol$^{-1}$, Fig. 1*A*) was obtained as a sodium salt (FEW Chemicals) and used as received. The individual light-harvesting nanotubes, consisting of double-walled nanotubular dye aggregates, were prepared in water/methanol as described in ref. 29. Solutions of light-harvesting nanotubes were stored in the dark and used for experiments within 3 d and up to 3 mo of preparation, respectively.

**Absorption Spectroscopy.** Absorption spectra from the solution were taken with a double-beam UV-visible spectrometer (Shimadzu UV-2101PC) in a 0.2-mm demountable quartz cell (oxidation experiments) and a 10-mm quartz cell (flash-dilution experiments), both cells from Hellmar GmbH.

**Cryo-EM.** Cryo-sample preparation, cryo-EM, and cryo-ET were performed as previously described (50) with only minor modifications. Briefly, 300-mesh copper grids covered with lacey holey carbon film (EMS) were hydrophilized before use by storing the grids over a water bath for 1 d. Droplets of the sample solution (5 μL) were applied to the grids and excess fluid was removed with filter paper until an ultrathin layer of the sample solution was obtained spanning the holes of the carbon film. The samples were then immediately vitrified by plunging the grid into liquid ethane close to its freezing point (90 K) using a guillotine-like plunging device. Rapidly frozen grids were stored in liquid nitrogen until examined by EM.

Cryo-samples were transferred into a Tecnai F20 transmission electron microscope (FEI, Inc.) using a Gatan cryoholder and transfer station (model 626; Gatan). Using the microscope control software SerialEM (51) single-axis tilt series were recorded at 200 kV in low-dose mode by rotating the sample from –60 to 60° in 2.0° angular increments. The total accumulated electron dose was limited to ~80 e/Å$^2$. A defocus of –8 μm was chosen to increase the contrast of the EM images. The magnification was 25,000 with a final pixel size of 4.54 Å. The software package IMOD (52) was used for fiducial alignment, tomogram reconstruction, and visualization by isosurface rendering (Fig. 2). The generation of nanotubes was not compatible with the widely used addition of colloidal gold fiducial marker; therefore, we used internal features presented in the tilt series as fiducial markers. The software PEET (Particle Estimation for Electron Tomography) (53) was used for subtomogram averaging with missing wedge correction of the nanotubes.

**Flash Dilution of Light-Harvesting Nanotubes in Solution.** A flash-dilution technique was performed as previously described (31) but with modifications. A water/methanol solution (~1 mL, concentration equal to the neat nanotube solution) was placed into a 4-mm quartz cell (Starna Cells, Inc.) while stirring the solution using a polytetrafluoroethylene (Teflon)-coated stir bar and magnetic stir plate. A small amount of the neat nanotube solution (~0.05 mL, $c_{C8S3} = 3 \times 10^{-4}$ mol·L$^{-1}$) was abruptly added to the stirring water/methanol solution (to render a final dye concentration of $c_{C8S3} = 8 \times 10^{-7}$ mol·L$^{-1}$). Transmission spectra were recorded on a custom-build fast-acquisition absorption spectrometer. A broadband quartz tungsten halogen source (66880; Newport/Oriel) was collimated, passed through the sample, and focused into a combination spectrometer/camera (Acton SP2500/Pixis 1024; Princeton Instruments). Spectra were collected in 10-ms bins starting immediately before flash dilution and then continuously for ~20 min. Absorption spectra were generated by combining sample transmission spectra to an initial reference spectrum.

**Two-Dimensional Spectroscopy.** Polarization-controlled 2D ES performed as previously described (54) but with modifications. A noncollinear parametric amplifier (NOPA) is pumped by a regeneratively amplified Ti:sapphire laser (Coherent Libra) at 800 nm with 350 μJ per pulse at 10 kHz. The NOPA generates pulses with a central wavelength of 590 nm and a full width at half maximum of 25 nm. A prism pair then compresses the pulses to ~30 fs. After the NOPA, the beam passes through a 2D phase mask (Tessera, $\lambda_c = 600$ nm, 20-μm spacing) optimized for first-order diffraction to produce four beams in the BOXCARS geometry. The beams are temporally controlled by a diffraction-based pulse shaper with a 2D spatial light modulator (SLM) (X7550; Hamamatsu). In the pulse shaper, the beams are spectrally dispersed by a ruled grating (900 grooves/mm, 550 nm blaze; Richardson) and imaged at different vertical positions by a cylindrical lens onto the SLM for independent temporal shaping. After pulse shaping, each beam is passed through a half wave plate (0.5 in, 600 nm AR-coated; Tower Optical) for individual polarization control. The beams are imaged from the phase mask to the sample position where the energy of each is ~100–200 pJ per pulse. The generated third-order polarization is then heterodyne-detected by spectral interferometry in a spectrometer (Acton SP2300, 300 grooves per millimeter grating, Pixis 400 camera; Princeton Instruments). The C8S3 solutions (dye concentration of $c_{C8S3} = 3.36 \times 10^{-4}$ mol·L$^{-1}$) are flowed through a 0.01-mm continuous-flow cell (Starna Cells) by a dual syringe pump (Ne-1000X ; New Age Pump Systems) at a rate of 6 mm/min.

**Chemical Oxidation of Light-Harvesting Nanotubes in Solution.** Oxidation chemistry was performed as previously described (31, 43, 46, 47) only with minor modifications. To a 400-μL nanotube solution was added 11 μL of 10 mM $AgNO_3$ solution. Absorption spectra were taken within 90 min of adding $AgNO_3$.

**Simulations.** The molecular arrangement for the double-walled LHNTs' inner cylinders is obtained by wrapping in a seamless way a 2D extended herringbone lattice (31) around a cylindrical surface. The collective optical excitations (excitons) are obtained from numerical diagonalization of a Frenkel exciton Hamiltonian, which accounts for the molecular transition energies and resonance interactions between the molecules. Linear spectra are calculated from the exciton eigen states using Fermi's golden rule. All steps involved are well-documented in the literature (23). Values for most of the model parameters are taken from the literature (ref. 31 and references therein); the remaining parameters are determined through comparison with the experimental spectra. For simulations with disorder to obtain extent of delocalization, we used uncorrelated energy disorder with a Gaussian distribution and a width of 250 cm$^{-1}$.

**Exciton Dynamic Simulations in 2D Morphology.** As a thought experiment, we investigate a simulation of the coherent exciton dynamics on a 2D elongated sheet. We construct a Frenkel exciton Hamiltonian that contains diagonal site energies and off-diagonal intermolecular transfer couplings for a bricklayer structure (*SI Appendix*, section 9). The site energies in the Hamiltonian are periodically modulated along to the short side of the sheet, which leads to a concentration of the exciton dynamics along the long side of the sheet. We simulate the coherent dynamics based on Schrödinger's equation generated by this Hamiltonian for the single-exciton state $|\psi\rangle$. The initial state is chosen to be at the center of the sheet. We observe the populations $|\langle m|\psi\rangle|^2$ of the different sites, where the corresponding single exciton states are $|m\rangle$. The dynamics of the cylindrical morphology shows only minimal differences.

**ACKNOWLEDGMENTS.** This work was primarily supported by the Department of Energy (DOE) through the DOE Center for Excitonics (an Energy Frontiers Research Center funded by the US DOE, Office of Science, Office of Basic Energy Sciences through Grant DE-SC0001088). D.M.E., D.H.A., C.P.S., R.A.J., K.A.N., and M.G.B. were supported as part of the DOE Center for Excitonics. D.M.E. was also supported in part by the Feodor Lynen Research Fellowship from the Alexander von Humboldt Foundation. D.N. acknowledges funding of the Brandeis electron microscopy facility and the facility manager, Dr. Chen Xu, by National Institutes of Health Grant P01GM062580 and National Science Foundation (NSF) Grant 0722582 (to D.N.). C.P.S. acknowledges support from an NSF Graduate Research Fellowship. A.T. acknowledges funding by the NSF (CHE-1212557). P.R. and S.L. acknowledge support from the Defense Advanced Research Projects Agency.

1. Scholes GD, Rumbles G (2006) Excitons in nanoscale systems. *Nat Mater* 5(9): 683–696.
2. Engel GS, et al. (2007) Evidence for wavelike energy transfer through quantum coherence in photosynthetic systems. *Nature* 446(7137):782–786.
3. Collini E, et al. (2010) Coherently wired light-harvesting in photosynthetic marine algae at ambient temperature. *Nature* 463(7281):644–647.
4. Scholes GD, Fleming GR, Olaya-Castro A, van Grondelle R (2011) Lessons from nature about solar light harvesting. *Nat Chem* 3(10):763–774.
5. Jendrny M, Aartsma TJ, Köhler J (2012) Fluorescence excitation spectra from individual chlorosomes of the green sulfur bacterium chlorobaculum tepidum. *J. Phys. Chem. Lett* 3:3745–3750.
6. Böhm PS, Southall J, Cogdell RJ, Köhler J (2013) Single-molecule spectroscopy on RC-LH1 complexes of Rhodopseudomonas acidophila strain 10050. *J Phys Chem B* 117(11): 3120–3126.
7. Orf GS, Blankenship RE (2013) Chlorosome antenna complexes from green photosynthetic bacteria. *Photosynth Res* 116:315–331.

8. Shibata Y, Saga Y, Tamiaki H, Itoh S (2009) Anisotropic distribution of emitting transition dipoles in chlorosome from Chlorobium tepidum: Fluorescence polarization anisotropy study of single chlorosomes. *Photosynth Res* 100(2):67–78.
9. Furumaki S, et al. (2011) Absorption linear dichroism measured directly on a single light-harvesting system: The role of disorder in chlorosomes of green photosynthetic bacteria. *J Am Chem Soc* 133(17):6703–6710.
10. Tian Y, et al. (2011) Organization of bacteriochlorophylls in individual chlorosomes from Chlorobaculum tepidum studied by 2-dimensional polarization fluorescence microscopy. *J Am Chem Soc* 133(43):17192–17199.
11. Sundström V, Pullerits T, van Grondelle R (1999) Photosynthetic light-harvesting: reconciling dynamics and structure of purple bacterial LH2 reveals function of photosynthetic unit. *J Phys Chem B* 103:2327–2346.
12. Hoeben FJM, Jonkheijm P, Meijer EW, Schenning APHJ (2005) About supramolecular assemblies of pi-conjugated systems. *Chem Rev* 105(4):1491–1546.
13. Frenkel J (1931) On the transformation of light into heat in solids II. *Phys Rev* 37:1276–1294.
14. Brédas JL, Beljonne D, Coropceanu V, Cornil J (2004) Charge-transfer and energy-transfer processes in pi-conjugated oligomers and polymers: A molecular picture. *Chem Rev* 104(11):4971–5004.
15. Balaban TS (2005) Tailoring porphyrins and chlorins for self-assembly in biomimetic artificial antenna systems. *Acc Chem Res* 38(8):612–623.
16. Lin H, et al. (2010) Collective fluorescence blinking in linear J-aggregates assisted by long-distance exciton migration. *Nano Lett* 10(2):620–626.
17. van Dijk L, Bobbert PA, Spano FC (2010) Extreme sensitivity of circular dichroism to long-range excitonic couplings in helical supramolecular assemblies. *J Phys Chem B* 114(2):817–825.
18. Akselrod GM, Walker BJ, Tisdale WA, Bawendi MG, Bulovic V (2012) Twenty-fold enhancement of molecular fluorescence by coupling to a J-aggregate critically coupled resonator. *ACS Nano* 6(1):467–471.
19. Aida T, Meijer EW, Stupp SI (2012) Functional supramolecular polymers. *Science* 335(6070):813–817.
20. Sarovar M, Whaley B (2013) Design principles and fundamental trade-offs in biomimetic light harvesting. *New J Phys* 15:013030.
21. Balaban TS, Tamiaki H, Holzwarth AR (2005) Chlorins programmed for self-assembly. *Supermolecular Dye Chemistry*, Topics in Current Chemistry, ed. Wuerthner F (Springer, Berlin), Vol 258, pp 1–38.
22. Knapp EW (1984) Vibrational line shapes in liquids. The role of resonant intermolecular coupling. *Chem Phys* 85:73–82.
23. Fidder H, Knoester J, Wiersma DA (1991) Optical properties of disordered molecular aggregates: A numerical study. *J Chem Phys* 95:7880–7890.
24. Ketelaars M, Kohler J, Aartsma TJ, Schmidt J, Schmidt J, van Oijen AM (1999) Unraveling the electronic structure of individual photosynthetic pigment-protein complexes. *Science* 285(5426):400–402.
25. Didraga C, Klugkist JA, Knoester J (2002) Optical properties of helical cylindrical molecular aggregates: The homogeneous limit. *J Phys Chem B* 106:11474–11486.
26. Didraga C, et al. (2004) Structure, spectroscopy and microscopic model of tubular carbocyanine dye aggregates. *J Phys Chem B* 108:14976–14985.
27. Rebentrost P, et al. (2008) Environment-assisted quantum transport. *New J Phys* 11:033003.
28. de Greef TFA, Meijer EW (2008) Materials science: Supramolecular polymers. *Nature* 453(7192):171–173.
29. Eisele DM, Knoester J, Kirstein S, Rabe JP, Vanden Bout DA (2009) Uniform exciton fluorescence from individual molecular nanotubes immobilized on solid substrates. *Nat Nanotechnol* 4(10):658–663.
30. Collini E, Scholes GD (2009) Coherent intrachain energy migration in a conjugated polymer at room temperature. *Science* 323(5912):369–373.
31. Eisele DM, et al. (2012) Utilizing redox-chemistry to elucidate the nature of exciton transitions in supramolecular dye nanotubes. *Nat Chem* 4(8):655–662.
32. Najafov H, Lee B, Zhou Q, Feldman LC, Podzorov V (2010) Observation of long-range exciton diffusion in highly ordered organic semiconductors. *Nat Mater* 9(11):938–943.
33. Renger T, Müh F (2013) Understanding photosynthetic light-harvesting: A bottom up theoretical approach. *Phys Chem Chem Phys* 15(10):3348–3371.
34. Pšencík J, et al. (2013) Structural and functional roles of carotenoids in chlorosomes. *J Bacteriol* 195(8):1727–1734.
35. Treat ND, et al. (2013) Microstructure formation in molecular and polymer semiconductors assisted by nucleation agents. *Nat Mater* 12(7):628–633.
36. Diao Y, et al. (2013) Solution coating of large-area organic semiconductor thin films with aligned single-crystalline domains. *Nat Mater* 12(7):665–671.
37. Kim BG, et al. (2013) A molecular design principle of lyotropic liquid-crystalline conjugated polymers with directed alignment capability for plastic electronics. *Nat Mater* 12(7):659–664.
38. Wang J, Brune DC, Blankenship RE (1990) Effects of oxidants and reductants on the efficiency of excitation transfer in green photosynthetic bacteria. *Biochim Biophys Acta* 1015(3):457–463.
39. Frese R, et al. (1997) The organization of bacteriochlorophyll c in chlorosomes from chloroflexus aurantiacus and the structural role of carotenoids and protein. *Photosynth Res* 54:115–126.
40. De Rossi U, et al. (1995) Control of the J-aggregation phenomenon by variation of the N-alkyl-substituents. *J Prakt Chem* 337:203–208.
41. von Berlepsch H, Kirstein S, Hania R, Pugzlys A, Böttcher C (2007) Modification of the nanoscale structure of the J-aggregate of a sulfonate-substituted amphiphilic carbocyanine dye through incorporation of surface-active additives. *J Phys Chem B* 111(7):1701–1711.
42. Clark KA, Krueger EL, Vanden Bout DA (2014) Direct measurement of energy migration in supramolecular carbocyanine dye nanotubes. *J Phys Chem Lett* 5(13): 2274–2282.
43. Eisele DM, et al. (2010) Photoinitiated growth of sub-7 nm silver nanowires within a chemically active organic nanotubular template. *J Am Chem Soc* 132(7):2104–2105.
44. Eisfeld A, Briggs JS (2002) The J-band of organic dyes: Lineshape and coherence length. *Chem Phys* 281:61–70.
45. Midgley PA, Dunin-Borkowski RE (2009) Electron tomography and holography in materials science. *Nat Mater* 8(4):271–280.
46. Lyon JL, et al. (2008) Spectroelectrochemical investigation of double-walled tubular J-aggregates of amphiphilic cyanine dyes. *J Phys Chem C* 112:1260–1268.
47. Cone CW, et al. (2011) Singular value decomposition analysis of spectroelectrochemical redox chemistry in supramolecular dye nanotubes. *J Phys Chem C* 115:14978–14987.
48. Augulis R, Pugžlys A, van Loosdrecht PHM (2006) Exciton dynamics in molecular aggregates. *Phys Stat Sol C* 3(10):3400–3403.
49. Milota F, et al. (2013) Vibronic and vibrational coherences in two-dimensional electronic spectra of supramolecular J-aggregates. *J Phys Chem A* 117(29):6007–6014.
50. Nicastro D, et al. (2011) Cryo-electron tomography reveals conserved features of doublet microtubules in flagella. *Proc Natl Acad Sci USA* 108(42):E845–E853.
51. Mastronarde DN (2005) Automated electron microscope tomography using robust prediction of specimen movements. *J Struct Biol* 152(1):36–51.
52. Kremer JR, Mastronarde DN, McIntosh JR (1996) Computer visualization of three-dimensional image data using IMOD. *J Struct Biol* 116(1):71–76.
53. Nicastro D, et al. (2006) The molecular architecture of axonemes revealed by cryoelectron tomography. *Science* 313(5789):944–948.
54. Turner DB, Nelson KA (2010) Coherent measurements of high-order electronic correlations in quantum wells. *Nature* 466(7310):1089–1092.